Visible light active, magnetically Fe_3O_4@SiO_2@TiO_2-Fe_2O_3 nanomaterial as photocatalyst for degraded phenol

Yuan Bai[a,b,*], Rui Ma[a], Xinwen Wan[a], Zongxian Jing[a], Jiayi Zhang[a]

[a]*School of Environment and Municipal Engineering, Lanzhou Jiaotong University, 730070 Lanzhou, China,*
Tel. 0086-9314956017; email: baiyuan@mail.lzjtu.cn (Y. Bai), Tel. 0086-15293100836; email: 491308356@qq.com (R. Ma),
Tel. 0086-13399460254; email: 1029506550@qq.com (X. Wan), Tel. 0086-18234000971; email: 215193156@qq.com (Z. Jing),
Tel. 0086-152 31098163; email: 840278825@qq.com (J. Zhang)
[b]*Key Laboratory of Yellow River Water Environment in Gansu Province, 730070 Lanzhou, China*

ABSTRACT

Magnetically and visible light active Fe_3O_4@SiO_2@TiO_2-Fe_2O_3 core-shell nanomaterial photocatalyst was successfully synthesized via the sol–gel anaerobic calcination approach. Transmission electron microscope (TEM), X-ray diffractometer, Fourier-transform infrared spectroscopy (FT-IR) and X-ray fluorescence spectrometer (XRF) were used to characterize the nanomaterial. For the samples heated to 600°C, XRF patterns demonstrated the presence of Fe, Si, Ti and O elements in Fe_3O_4@SiO_2@TiO_2-Fe_2O_3 composite, whereas TEM micrographs indicated crystalline structures and diffraction patterns and FT-IR measurement revealed weak peaks of Fe_3O_4@SiO_2@TiO_2-Fe_2O_3 at 3,441 cm^{-1}. When Fe_2O_3 was adsorbed on TiO_2, the band gap reduced and the iron oxide–TiO_2 showed photocatalytic activity in visible light region. To test their photocatalytic ability for phenol degradation rate under different experimental conditions such as different phenol concentration, various pH of the solution and amount of applied photocatalyst. The degradation conditions were determined by single-factor analysis, the photocatalytic reaction time was 300 min, it was found that the degradation rate was 35.07%, the pH value was 7 and 12, the degradation rate was 33.54% and 41.51%, phenol concentration was 3 mg/L, the degradation rate was 30.9%. As the intensity of xenon light increased, the photocatalytic activity declined. Hence these mentioned conditions were chosen as the optimum experimental conditions.

Keywords: Magnetic nanomaterial; Fe_3O_4@SiO_2@TiO_2-Fe_2O_3; Visible light; Photocatalysis; Phenol

1. Introduction

The poisonous organic contamination from various industrial operations and human activities has gradually turned into an intractable issue in environmental governance [1]. Organic species including phenol, etc. are toxic to humans, either being carcinogenic or affecting the physical-motor functioning of the body [2]. Phenol is discharged by many industries, including refineries and organic chemicals manufacturing, as it is used as a precursor and an intermediate [3]. Based on the type of pollutant source, the phenolic concentration of the effluent streams can reach up to hundreds or thousands of parts per million [4]. Domestic sewage and surface water runoffs from agricultural activities also allow phenols to find pathways to enter the ecosystem [5,6]. Furthermore, phenols are naturally found in tyrosine, one of the standard amino acids found in epinephrine (adrenaline), proteins and can also obtained from essential oils of plants [7]. Apart from

* Corresponding author.

established techniques such as chemical precipitation, biological treatment, adsorption, and so on, several techniques for the removal of organic and inorganic species have been studied recently, including chemical oxidation [8,9], electrochemical processes [10–12], membrane separation [13], sonochemical treatments [14,15], and coupling chemical oxidation processes with biological treatments [9,16]. All the techniques have certain challenges, either in terms of economics or ultimate safe disposal. Photocatalytic technology has been considered as an effective way for pollutants to be removed. TiO_2 has a pivotal role in the new environmental protection technology of photocatalysis due to its non-toxic, stable photocatalytic performance and low cost [17,18], compared with ZnO, SnO_2, ZrO_2, CdS and other semiconductor materials that have their own losses and toxicity [19–22].

The photocatalytic efficiency of the TiO_2 is limited due to the wide band gap (3.2 eV for anatase phase) of the TiO_2 needs ultraviolet light for the activation of the photocatalyst, and results in a minimum utilization of solar light. In the solar spectrum, only 5% of the sun's energy belongs to the UV range, while it is 45% for the visible range [23], its absorption is confined to the UV range, which indicates that about 2%–5% of the energy can only be utilized from the solar spectrum. Further, the ability of the photocatalytic activity of pristine TiO_2 is still low due to the poor rate of chemical interaction between TiO_2 and adsorbed pollutants compared to the rate of photogenerated electron–hole pairs in the system [24]. Doping of elements, noble metal deposition, morphology modification, the hybridization of metal oxide with other semiconductors, as well as incorporation with metalorganic frameworks are the most common strategies used for enhanced photocatalytic activity [25].

For instance, Tong et al. [26] designed a Si-α-Fe_2O_3/CdS composites by a hydrothermal method, which exhibited a photocatalytic activity for the degradation of 20 mg/L *p*-nitrophenol within 120 min with an efficiency of 66% under visible-light irradiation. A hetero-structure of defect-rich TiO_2 nanoparticles anchored in g-C_3N_4 had been prepared via a synchronous compound process combined with the pyrolysis of Ti-MOF and melamine, the optimal sample ($4TiO_2$/CN) exhibited the high photocatalytic activities for the degradation of phenol (1.63×10^2 μmol/g·h) [27]. CN-OvTiO_2 was synthesized via solvent evaporation deposition method, the results shows a high quantum yield of 0.15% at 500 nm monochromatic light and a high ammonia production rate of 34 μmol/g_{cat} under visible light irradiation, 8.5 times higher than that of pure CN, this work deeply reveals the link and synergy mechanism of heterojunction and defects [28]. The nanocomposite with weight a ratio of RGO to TiO_2 (37.0%–55.7%) had achieved maximum degradation of phenol from aqueous solution, and about 97.87% of phenol had been removed within 180 min under UV-light illumination [1].

Doping with transition metal elements in TiO_2 is attractive as their electronic configuration make them suitable for catalysis [29]. Mechanically, transition metal elements tend to replace Ti atom, leading to the hybridization with O2p and Ti3d orbitals, so the electronic structure and optical properties of TiO_2 can be modified [30]. The radius of Fe^{3+} ion (0.645 Å) is equivalent to that of Ti^{4+} ion (0.605 Å), so doping

Fe in TiO_2 lattice is allowed in principle. Doping of TiO_2 with Fe has shown interesting photocatalytic properties [30].

Magnetic material Fe_3O_4 has good dispersibility and can be used as a carrier for rapid recovery of photocatalytic materials [31,32]. However, the magnetic property of the Fe_3O_4 carrier will be destroyed under acidic conditions. If Fe_3O_4 and TiO_2 are in direct contact, an unpleasant heterojunction will occur, which will affect the electron–hole pair of TiO_2 and interfere with its utilization of light [33,34], so SiO_2 is selected as the intermediate layer because of its strong stability, biocompatibility and the ability to prevent particles from agglomeration [35].

In this work, Fe_3O_4 was used as the core material, and Fe_3O_4@SiO_2@TiO_2-Fe_2O_3 was successfully synthesized via the sol–gel anaerobic calcination approach. Characterizations of the Fe_3O_4@SiO_2@TiO_2-Fe_2O_3 were performed using transmission electron microscopy (TEM), X-ray diffraction (XRD), Fourier-transform infrared spectroscopy (FT-IR) and X-ray fluorescence spectrometer (XRF), the photocatalytic activities of Fe_3O_4@SiO_2@TiO_2-Fe_2O_3 to degrade phenol were studied under visible light.

2. Materials and methods

2.1. Chemicals and materials

The Unico UV-2100 Spectrophotometer was purchased from Beijing Boya Innovation Technology Co., Ltd., (China) was used for the determination of phenol concentration. Tecnai G2 TF20 field-emission transmission electron microscope (FEI Company, United States), was used to observe the morphology of the material. SmartLab SE Polycrystalline Powder X-ray diffractometer (Rigaku Corporation, Japan), Fourier-transform infrared spectroscopy (FT-IR, IFS66V/S, Bruker, Germany) and X-ray fluorescence spectrometer (XRF, MagixPW2403, PANalytical, United States), was used to determine the structure of photocatalytic particles.

The chemicals used in this study were of analytical grade. Iron(III) chloride hexahydrate ($FeCl_3 \cdot 6H_2O$), ferrous sulfate ($FeSO_4 \cdot 7H_2O$), ammonium hydroxide (NH_3), nanoscale ferric oxide (Fe_3O_4), sodium dodecylbenzene sulfonate ($C_{18}H_{29}NaO_3S$), tetraethyl orthosilicate ($C_8H_{20}O_4Si$), titanium tetrachloride ($TiCl_4$), ferric nitrate ($Fe(NO_3)_3$), ferrous sulfate ($FeSO_4$), concentrated hydrochloric acid (HCl), acetylacetone ($C_5H_8O_2$) were purchased from Yixin Corporation (Lanzhou, China). All the chemicals were used as received without further purification.

2.2. Experimental method

2.2.1. Preparation of Fe_3O_4 nanoparticles

The preparation of Fe_3O_4 nanoparticles adopted the co-precipitation method. The mixed solution of $FeCl_3 \cdot 6H_2O$:$FeSO_4 \cdot 7H_2O$ = 2:3 was added distilled water, and stirred for 2 h with a powerful mixer. The pH of the mixture was then adjusted to about 11–12 by using ammonia solution (25%–28%), Fe_3O_4 particles were obtained after 30 min of stirring, the precipitate was centrifuged at 4000 rpm for 5 min and washed with ethanol and deionized water several times (Fig. 1a). Finally, Fe_3O_4 nanoparticles were stored in ethanol for future usage.

2.2.2. Preparation of Fe₃O₄@SiO₂ magnetic particles

In order to prevent the aggregation and keep the magnetic properties of Fe_3O_4, the magnetic composite particles of $Fe_3O_4@SiO_2$ were prepared by the sol–gel method. Mixed 80 mL of anhydrous ethanol, 20 mL of sodium dodecylbenzene sulfonate, and 2.4 mL of concentrated ammonia, added 0.5 g Fe_3O_4 (pure material, without ethanol mass) magnetic particles, dissolved in an ultrasonic machine for 1h, then added 5 mL of ethyl orthosilicate, stirred for 6 h with a powerful mixer, the solvent was separated by the magnetic, washed with ethanol and deionized water for several times, and dried at 60°C. Finally, the magnetic composite nanoparticles of $Fe_3O_4@SiO_2$ were obtained after grinding and sieving (Fig. 1b).

2.2.3. Preparation of TiO₂-Fe₂O₃ sol

260 mL of deionized water, 50 mL of titanium tetrachloride solution mixed form 25 wt.% titanium tetrachloride solution, and maintained in cooling water for a subsequent operation, 0.599 g of ferric nitrate and 0.275 g of ferrous sulfate were dissolved in 60 mL of deionized water, 0.3 mL of concentrated hydrochloric acid solution was added into the aforesaid solutions, then ultrasonically processed for 30 s. The mixture liquid was marked as A. Filled the titanium tetrachloride solution in a 250 mL beaker. Stirred solution on the magnetic stirrer, at the same time dropped A, till all the A solution was dripped, continue stirred for 30 min, ammonia water was added to adjust the pH value to 1, after 30 min of stirring, added 1 mL acetylacetone solution to the sol as a fixative and stirred for 30 min. Placed in the oven for aging at a fixed temperature for 3 h. After aging, it was stirred for 30 min to form the catalyst sol.

2.2.4. Preparation of magnetic photocatalytic particles

0.5 g of $Fe_3O_4@SiO_2$ magnetic material and 20 mL of $TiO_2-Fe_2O_3$ sol were mixed, electrically stirred for 4 h, separated by a magnetic field, dried at 80°C and calcined at 600°C for 2 h. The final magnetic photocatalyst particles were obtained (Fig. 1c). The magnetic performance of the as-synthesized photocatalyst was investigated by Baye-801 Gaussmeter, and the magnetic Fe_3O_4 value was 0.50–0.55 g. The magnetic value of $Fe_3O_4@SiO_2$ was 0.40–0.45 g, and the magnetic value of $Fe_3O_4@SiO_2@TiO_2-Fe_2O_3$ was 0.10–0.15 g. However, the magnetic value of $Fe_3O_4@SiO_2@TiO_2-Fe_2O_3$ absorbed with phenol was 0.10–0.15 g, indicating that the magnetic particles had a certain magnetic force and could be recovered by high-strength magnets. In addition, the magnetic particles still had magnetic properties after phenol degradation, indicating that this material could be recycled.

2.3. Photocatalytic activity test

The photocatalytic activity of the samples was examined through the photocatalytic degradation of phenol under visible light irradiation. The source of visible light used xenon lamps. Every experiment was performed by adding 0.5 g of the samples to 100 mL of the phenol solution with an initial concentration of 10 mg/L. A stirrer was used to uniformly distribute the photocatalytic particles in the solution. The initial solution pH was adjusted using HCl and ammonium hydroxide. The phenol solutions were analyzed by recording the variations of the absorption band maxima at 510 nm using a UV spectrophotometer. A series of batch experiments were carried under various catalytic conditions, including catalyst dosage, initial phenol solution concentration, pH, and different ration of Fe:Ti, to investigate the $Fe_3O_4@SiO_2@TiO_2-Fe_2O_3$ reduction performances of the as-synthesized catalysts.

The photocatalytic performance was calculated using the following equation:

$$D\left(\%\right) = \frac{C_0 - C}{C_0} \times 100 \tag{1}$$

where C_0 and C, respectively, represent the phenol concentration at baseline and after light irradiation.

3. Results and discussion

3.1. Single-factor analysis

3.1.1. Effect of time on photocatalytic activity of Fe₃O₄@SiO₂@TiO₂-Fe₂O₃

Under optimum conditions of all other factors, the phenol solutions were subjected to visible irradiation for different time durations from 5 to 300 min. The degradation trend is given in Fig. 2a. As the time of degradation rate was increased, the degradation rates were 5.00%, 8.82%, 20.99%, 24.09%, 29.82%, 32.68%, 33.63% and 35.07%, respectively.

3.1.2. Effect of pH on photocatalytic activity of Fe₃O₄@SiO₂@TiO₂-Fe₂O₃

According to the previous researches, pH plays a significant role in the photodegradation of numerous organic contaminants [1]. pH may influence degradation of phenol, the surface charge of $TiO_2-Fe_2O_3$, and other physicochemical properties. The real effluent containing phenol can be discharged at various pH, thus a series of experiments were carried out to investigate the influence of pH on the degradation efficiency of phenol by varying the initial pH from 2 to 12 (Fig. 2b). The photocatalytic degradation efficiency of phenol by the $Fe_3O_4@SiO_2@TiO_2-Fe_2O_3$ nanohybrids decreased at pH of 2–7 and then increased at pH of 8–12, demonstrated that phenol photodegradation over $Fe_3O_4@SiO_2@TiO_2-Fe_2O_3$ was more favorable in strong alkaline conditions and strong acidic conditions, and the maximum degradation amount of phenol was obtained when pH was 12, which could be mostly attributed to the interaction/affinity between $TiO_2-Fe_2O_3$ and phenol.

3.1.3. Effect of phenol concentration on photocatalytic activity of Fe₃O₄@SiO₂@TiO₂-Fe₂O₃

The effect of initial phenol concentrations on the properties of the photocatalytic process was evaluated within the range of 3–7 mg/L. As shown in Fig. 2c, when the
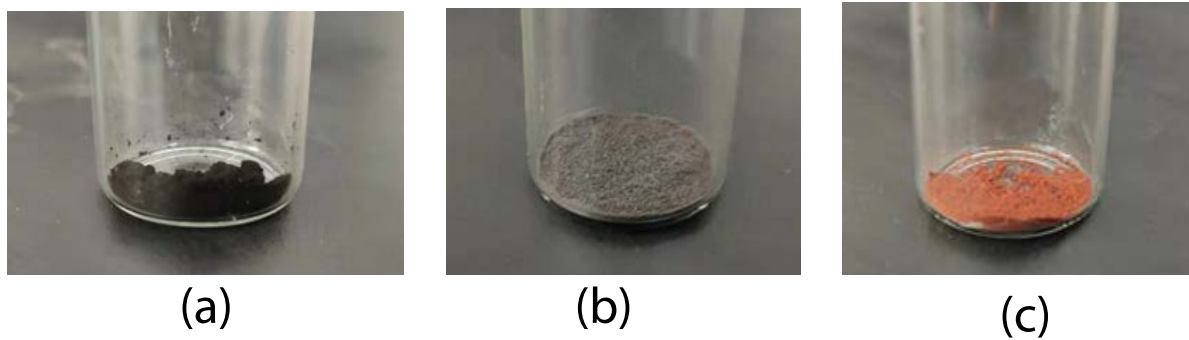
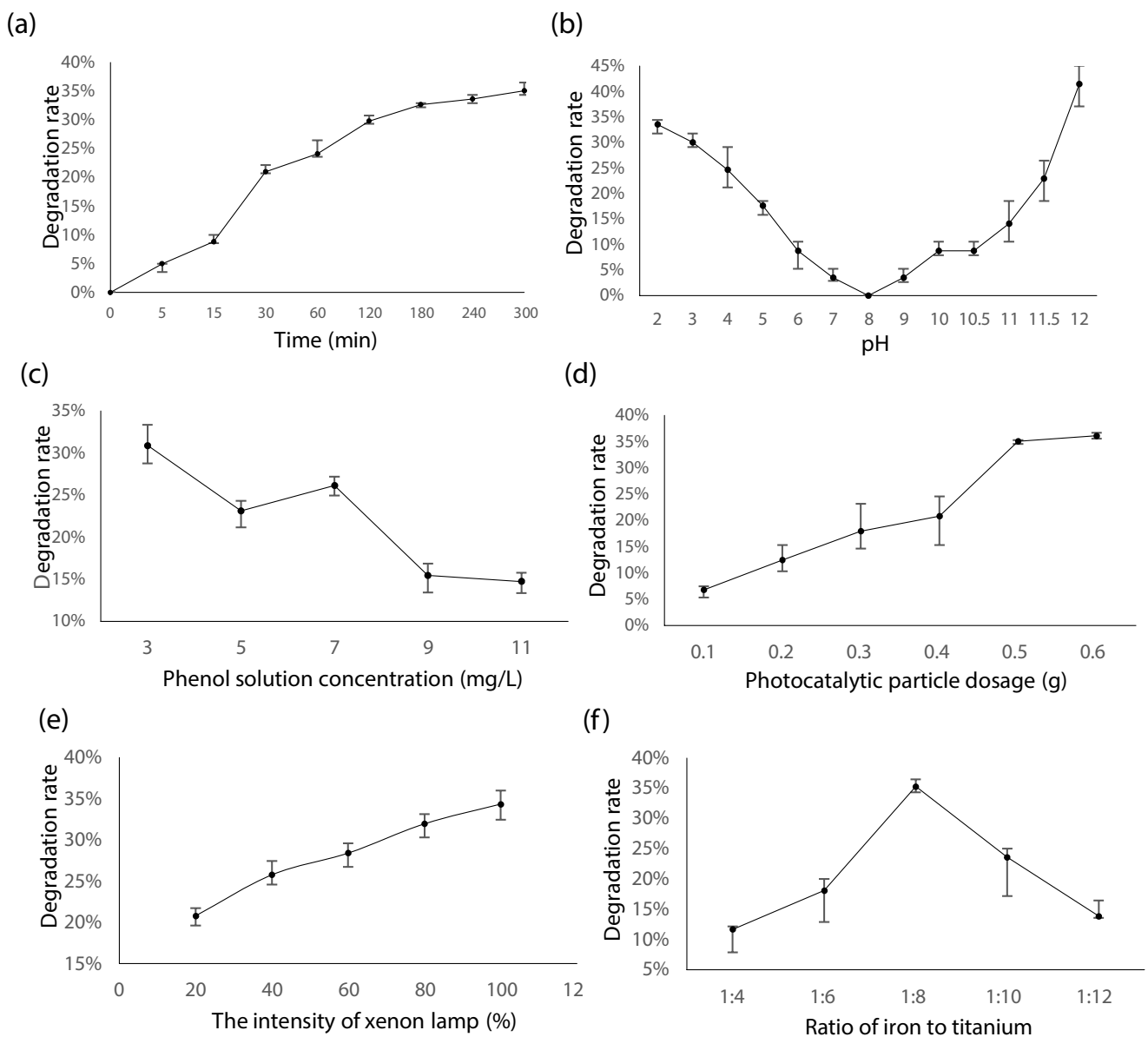(a)　　　　　　　　　(b)　　　　　　　　　(c)

Fig. 1. Magnetic photocatalytic particles.

Fig. 2. Photocatalytic degradation of phenol at single-factor analysis. Photocatalytic degradation of phenol on 0.1 g/100 mL $Fe_3O_4@SiO_2@TiO_2$-Fe_2O_3 samples at different (a) photocatalytic reaction time, (b) pH, (c) phenol solution concentration, (d) photocatalytic dosage, (e) intensity of xenon lamp, and (f) ration of iron to titanium.

photocatalyst dosage and reaction time were held constant (0.1 g/100 mL and 120 min), the photocatalytic efficiency gradually decreased as the initial phenol concentration increased. The concentration of phenol was 3 mg/L, the degradation rate reached to 30.9%. However, as the concentration increased to 9 mg/L, the degradation rate of phenol dropped to 15.44%. As shown in Fig. 2c, photodegradation changed with increasing the initial phenol concentration, which may be related to the light reaching the surface of photocatalyst and the amount of the pollutants on its surface balance. At the lower concentrations, adequate light passes over the catalyst surface throughout the solution, which results in photogenerated electron–holes creating hydroxyl radicals to degrade the contaminant. However, at the higher initial concentrations of pollutants, a large portion of the incoming light is blocked by pollutants causing reduced photogenerated electron–holes with lower electron excitation and decreased hydroxyl radicals. This phenomenon eventually decreases photocatalytic degradation performance, and therefore, higher photodegradation at lower contaminant concentrations was observed [36]. Furthermore, at high initial concentrations, with progress in the degradation, some intermediates will form and competitively adsorb on the surface of the photocatalyst and also react with oxidant species [37].

3.1.4. Effect of the dosage of photocatalyst particles on photocatalytic activity of $Fe_3O_4@SiO_2@TiO_2$-Fe_2O_3

The degradation efficiency of the catalyst is shown in Fig. 2d. With the increase of the amount of the catalyst, the degradation rate of the phenol solution was continuously increased. The degradation rate of the phenol solution was 6.79%, 12.49%, 17.95%, 20.81%, 35.07%, and 36.12%, respectively. When the amount of the catalyst was 0.1 g the amount of the catalyst contained in the solution per unit volume was limited, which could not generate enough photoelectron–hole pairs, and the contact chance between the phenol molecules and the catalyst was less, when the amount of catalyst added was 0.5 g, the conversion of phenol reached 35.07% and tended to be stable. The reason is that the increase of photocatalyst will provide more reactive sites initially, which can facilitate the removal efficiency, while the overmuch photocatalysts may result in the lack of light penetration, thereby decreasing the degradation rate [38,39].

3.1.5. Effect of illumination intensity of xenon lamp on photocatalytic activity of $Fe_3O_4@SiO_2@TiO_2$-Fe_2O_3

0.2 g of magnetic photocatalytic particles were added into 200 mL of phenol solution, with the concentration of phenol solution at 1 mg/L. After ultrasonic shock for 1 min. Phenol removal efficiency for the intensity of xenon lamp was depicted in Fig. 2e, xenon lamp intensity was 100% and illumination was 2 h. The degradation rate of phenol was 34.35%, the intensity of xenon lamp was reduced to 80%, and the degradation rate of phenol was reduced to 31.98%. The intensity of xenon lamp was reduced to 20%, and the degradation rate of phenol reached 20.81%. It indicated that the intensity of the xenon lamp affected the degradation rate of magnetic photocatalytic particles for phenol in

phenol solution. With the lower intensity of the xenon lamp, the degradation rate was lower.

3.1.6. Effect ration of Fe to Ti on photocatalytic activity of $Fe_3O_4@SiO_2@TiO_2$-Fe_2O_3

The magnetic particle catalysts with the ratio of Fe to Ti with 1:4, 1:6, 1:10, and 1:12 were prepared at a calcination temperature of 600°C, and an aging temperature of 80°C for 3 h.

Fig. 2f shows the degradation rate was relatively low at the Fe:Ti of 1:4, 1:6, 1:8, 1:10, and 1:12, and the difference was not significant. Moreover, due to the greater Fe:Ti being favorable to the magnetic particles, the rate of degradation of the magnetic photocatalytic particles in the phenol solution tended to rise with the continual lowering of the quantity of Fe_3O_4. More TiO_2 was applied to the magnetic core, which enhanced the photocatalytic activity and accelerated the phenol solution degradation. The degradation rate sharply increased when the Fe:Ti ratio dropped from 1:4 to 1:8. However, the degradation rate started to decrease when the Fe:Ti ratio was altered to 1:10, Banisharif et al. [40] studied the photocatalytic conversion of TCE on pure TiO_2 and 0.05%–0.5% Fe_2O_3-TiO_2 on 0.5 g photocatalyst under UV irradiation. The results showed that 0.1 wt.% Fe_2O_3-doped TiO_2 sample dried at 100°C showed a maximum photocatalytic TCE conversion of about 97% with minor amounts of CO as a hazardous by-product. Fe_2O_3 addition to TiO_2 sharply suppresses the degradation activity of the photocatalysts. The photocatalytic activity of Fe–Ti mixed oxides for degradation of toxic compounds in water also showed the same behavior as the maximum activity at an optimum concentration of iron oxide dopant [41]. The optimal Fe:Ti should be controlled at about 1:8.

3.2. TEM characterization analysis

In Fig. 3a Fe_3O_4 nanoparticles had small and uniform particle sizes, with an average particle size of 100nm and good single dispersion. In the preparation of $Fe_3O_4@SiO_2$ magnetic particles, Fe_3O_4 magnetic nanoparticles were prone to agglomeration, and liquid phase reaction, which had some limitations. During the reaction process, the nuclei were slightly agglomerated and there was no obvious dividing line between the core and shell structures. In Fig. 3b a layer of SiO_2 was attached to the surface of Fe_3O_4, which increased the overall particle size to about 150 nm, and there was obvious dispersion between $Fe_3O_4@SiO_2$ particles, indicated that the addition of SiO_2 layer did not change the surface morphology of Fe_3O_4 magnetic particles, but only formed a protective core-shell structure on Fe_3O_4. In Fig. 3c the addition of TiO_2-Fe_2O_3 made certain agglomeration phenomena occur on the surface of $Fe_3O_4@SiO_2$ core-shell structure, and TiO_2 surface was smooth and attached to $Fe_3O_4@SiO_2$ particles. TiO_2-Fe_2O_3 layer increased the specific surface area of the entire magnetic particle layer. The introduction of titanium ions caused hydrolytic condensation on the surface of $Fe_3O_4@SiO_2$, and titanium oligomers were formed on the surface of TiO_2-Fe_2O_3 under the action of –OH on the surface of SiO_2. Finally, titanium oligomers develop into TiO_2 shells of different thicknesses
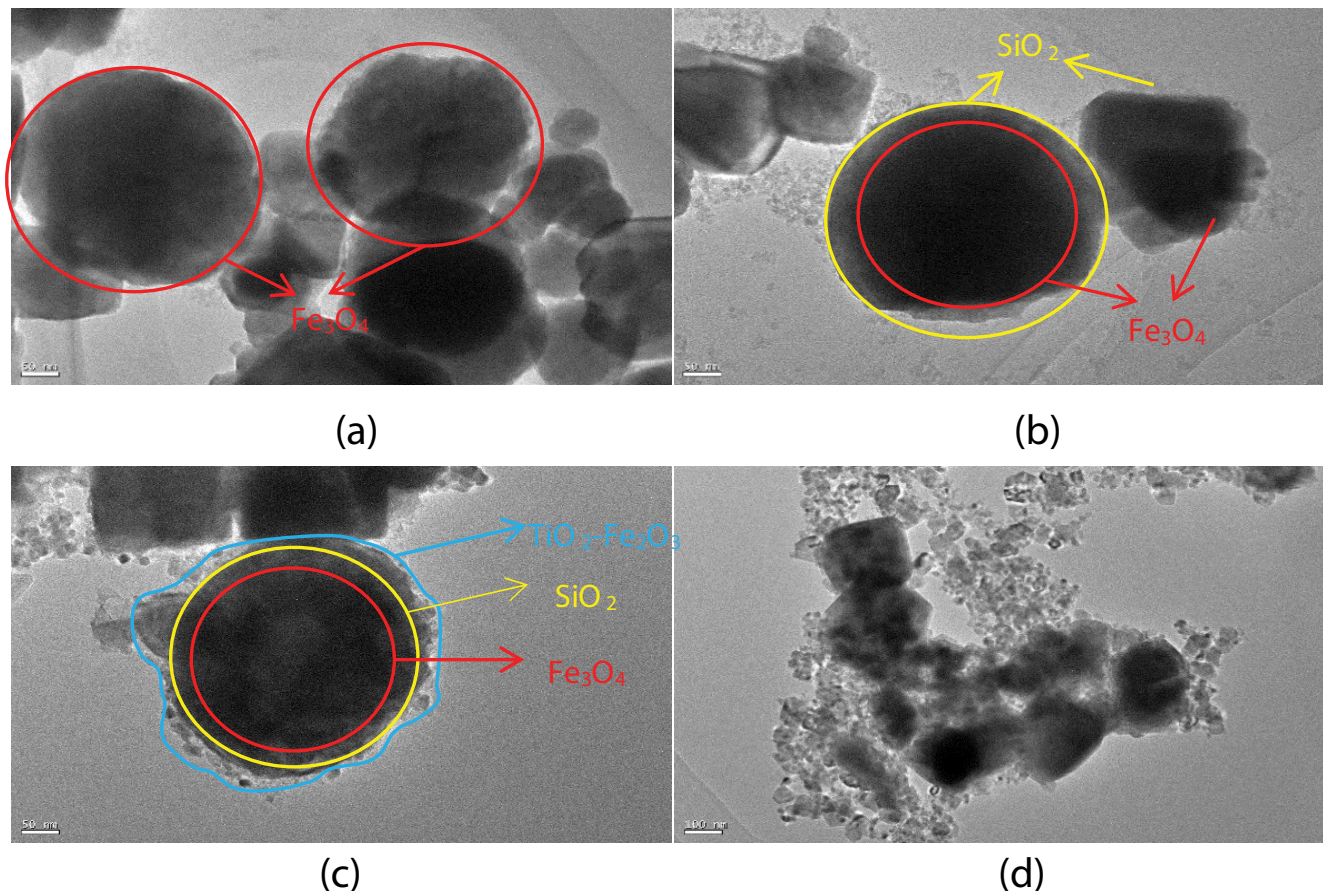
Fig. 3. TEM images of Fe_3O_4, Fe_3O_4@SiO_2, Fe_3O_4@SiO_2@TiO_2-Fe_2O_3 magnetic particles and Fe_3O_4@SiO_2@TiO_2-Fe_2O_3 for photocatalytic reaction.

through homogeneous nucleation, and formed Fe_3O_4@SiO_2@TiO_2-Fe_2O_3 magnetic particles. Fig. 3d shows that Fe_3O_4@SiO_2@TiO_2-Fe_2O_3 magnetic particles absorbed a portion of the substances in the phenol solution after entering the phenol solution via photocatalytic reaction, which changed the surface of the magnetic particles and increased the specific surface area. It was proved that phenol was degraded by Fe_3O_4@SiO_2@TiO_2-Fe_2O_3 magnetic particles.

3.3. XRD characterization analysis

XRD was used to characterize the structural properties of Fe_3O_4, Fe_3O_4@SiO_2, Fe_3O_4@SiO_2@TiO_2-Fe_2O_3, and phenol degradation.

Fig. 4a is the XRD pattern of Fe_3O_4 powder, where the diffraction peaks at $2\theta = 35.62°$ correspond to the (311) diffraction peaks of cubic Fe_3O_4 (PDF # 75-0449), and the other series of diffraction peaks of the Fe_3O_4 phase map one by one, such as (220), (400), (511) and (440). These results indicate that Fe_3O_4 powder had been successfully synthesized.

Fig. 4b is the XRD pattern of the Fe_3O_4-coated SiO_2 powder (Fe_3O_4@SiO_2), where the wide diffraction peaks at $2\theta = 12.60°$ correspond to the characteristic peak of SiO_2 (PDF # 82-1564). These results indicate that SiO_2 was formed on the surface of Fe_3O_4 and Fe_3O_4@SiO_2 samples were successfully prepared.

The Fe_3O_4@SiO_2 powder coated with TiO_2-Fe_2O_3 (Fe_3O_4@SiO_2@TiO_2-Fe_2O_3) is shown in Fig. 4c. Two distinct diffraction peaks appeared at $2\theta = 27.84°$ and $2\theta = 54.88°$, which correspond to the (110) and (211) diffraction peaks of tetragonal TiO_2 (PDF # 82-0514). Due to the (101) peak of the tetragonal phase TiO_2-Fe_2O_3 coincided with the (311) diffraction peak of the cubic phase Fe_3O_4 at $2\theta = 35.62°$, the strength of the peak of Fe_3O_4@SiO_2@TiO_2-Fe_2O_3 was obviously enhanced, and Fe_3O_4@SiO_2@TiO_2-Fe_2O_3 samples were successfully prepared.

The prepared Fe_3O_4@SiO_2@TiO_2-Fe_2O_3 sample's XRD pattern is displayed in Fig. 4d after it participated in the phenol reaction, the results demonstrated that the Fe_3O_4@SiO_2@TiO_2-Fe_2O_3 samples did not clearly undergo phase transformation during the reaction, and had a good stability phase structure.

3.4. FT-IR characterization analysis

The change of a functional group or bond of Fe_3O_4, Fe_3O_4@SiO_2, Fe_3O_4@SiO_2@TiO_2-Fe_2O_3 and degradation of phenol were characterized by FT-IR depicted in Fig. 5. Fe_3O_4, Fe_3O_4@SiO_2 and Fe_3O_4@SiO_2@TiO_2-Fe_2O_3 had a weak absorption peak at 3,439; 3,413 and 3,441 cm^{-1}, respectively, which could be attributed to the absorption peak of the association
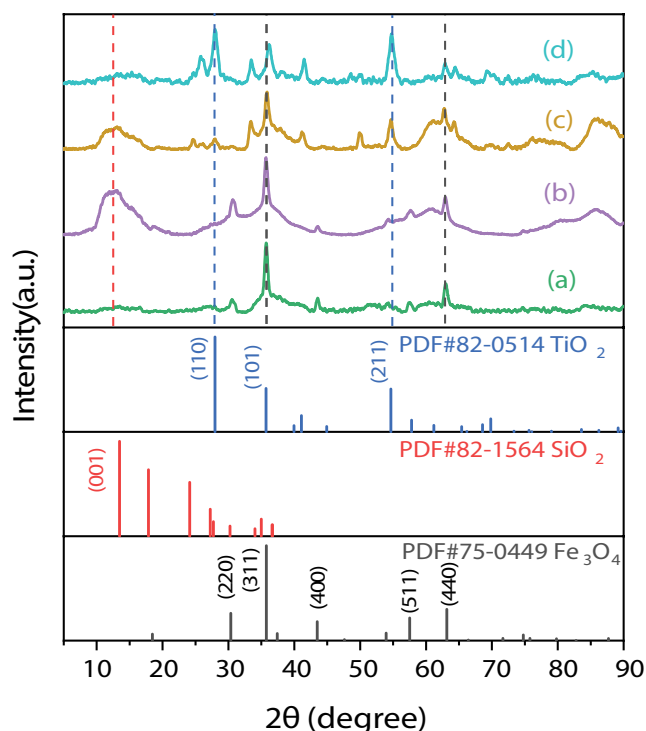
Fig. 4. XRD of $Fe_3O_4@SiO_2@TiO_2-Fe_2O_3$ magnetic particles.

Fig. 5. FT-IR of $Fe_3O_4@SiO_2@TiO_2-Fe_2O_3$ magnetic particles and degradation of phenol.

hydroxyl group, it showed that the material had certain water absorption in the air. Similarly, the weak absorption peaks of the three samples at 1,640 cm^{-1} could be attributed to the flexural vibration absorption peaks of the O–H adsorbed water on the surface of the material, which showed that the sample had a certain degree of water absorption in the air, and the surface was easy to carry a certain amount of hydroxyl. In the infrared spectra of Fe_3O_4 nanoparticles, the strong absorption peak at 551 cm^{-1} was the characteristic absorption peak of Fe–O in Fe_3O_4. In the infrared spectra of $Fe_3O_4@SiO_2$, the absorption peak near 1,067 cm^{-1} was attributed to the stretching vibration absorption peak of Si–O–Si bond, and the absorption peak near 799 cm^{-1} was attributed to the antisymmetric stretching vibration absorption peak of Si–O–Si bond, the absorption peak at 568 cm^{-1} was the characteristic absorption peak of Fe–O–Si. The results showed that a layer of SiO_2 was successfully coated on the surface of Fe_3O_4 nanoparticles, and instead of being deposited on the surface of Fe_3O_4 by physical adsorption, the Fe–O–Si bond was formed and the SiO_2 was bonded to the surface of Fe_3O_4 by chemical bond. In the $Fe_3O_4@SiO_2@TiO_2-Fe_2O_3$ composite, the absorption peak of 714 cm^{-1} was the stretching vibration absorption peak of Ti–O–Ti bond, and the absorption peak of 910–960 cm^{-1} belonged to the stretching vibration absorption peak of Ti–O–Si. The results showed that the bond between SiO_2 and TiO_2 was effective. The locations of these peaks depended on the chemical composition of the sample, and the contents of each component determined the strength of the correlated peaks. It was known from the literature that the presence of Ti–O–Si bond could strengthen the acidity of the surface of the composite, which was conducive to the formation of stronger
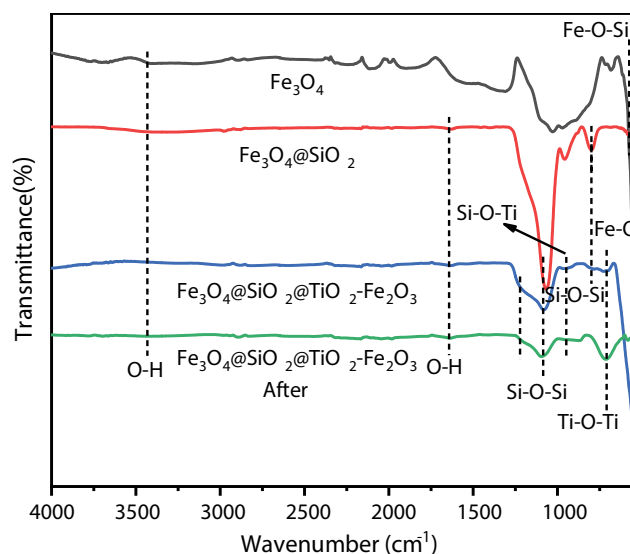
surface free radicals, the photocatalysis activity of the composite could be enhanced by redox with the organic matter adsorbed on the surface of the composite, which inhibited electron-hole recombination [42,43]. Nevertheless, excessive Ti–O–Si bond would lead to the formation of hole and electron recombination center, reduced the photocatalytic activity. The positions of the absorption peaks in the infrared spectra of the recycled materials after degradation of phenol were approximately the same as before, but the strength of Si–O–Si, Ti–O–Si and Ti–O–Ti bonds altered moderately, and the strength of Ti–O–Si and Si–O–Si bonds declined after degradation, the strength of Ti–O–Ti bond increased, which may be due to the interaction with phenol during degradation.

3.5. XRF characterization analysis

In order to investigate the distribution of elements of Fe_3O_4, $Fe_3O_4@SiO_2$, $Fe_3O_4@SiO_2@TiO_2-Fe_2O_3$ and degradation of phenol nanocomposites, the XRF was performed. The XRF results of the support and nanocatalyst are shown in Fig. 6a–d, respectively.

The presence of elements included Fe, Si, Ti and O elements in $Fe_3O_4@SiO_2@TiO_2-Fe_2O_3$ composite. Additionally, the presence of elements confirmed that the catalyst was successfully prepared. The Si/Ti ratio of the composites changed before and after the degradation of phenol, which was consistent with the results of FT-IR analysis.

3.6. Catalytic mechanism analysis

$Fe_3O_4@SiO_2@TiO_2-Fe_2O_3$ magnetic photocatalytic particles formed Ti–O–Si bond, which enhanced the acidity of the surface of the composite, particles were conducive to the formation of stronger surface free radicals, which received light-induced holes and redox with the organic matter adsorbed on the surface of the composite, the electron–hole
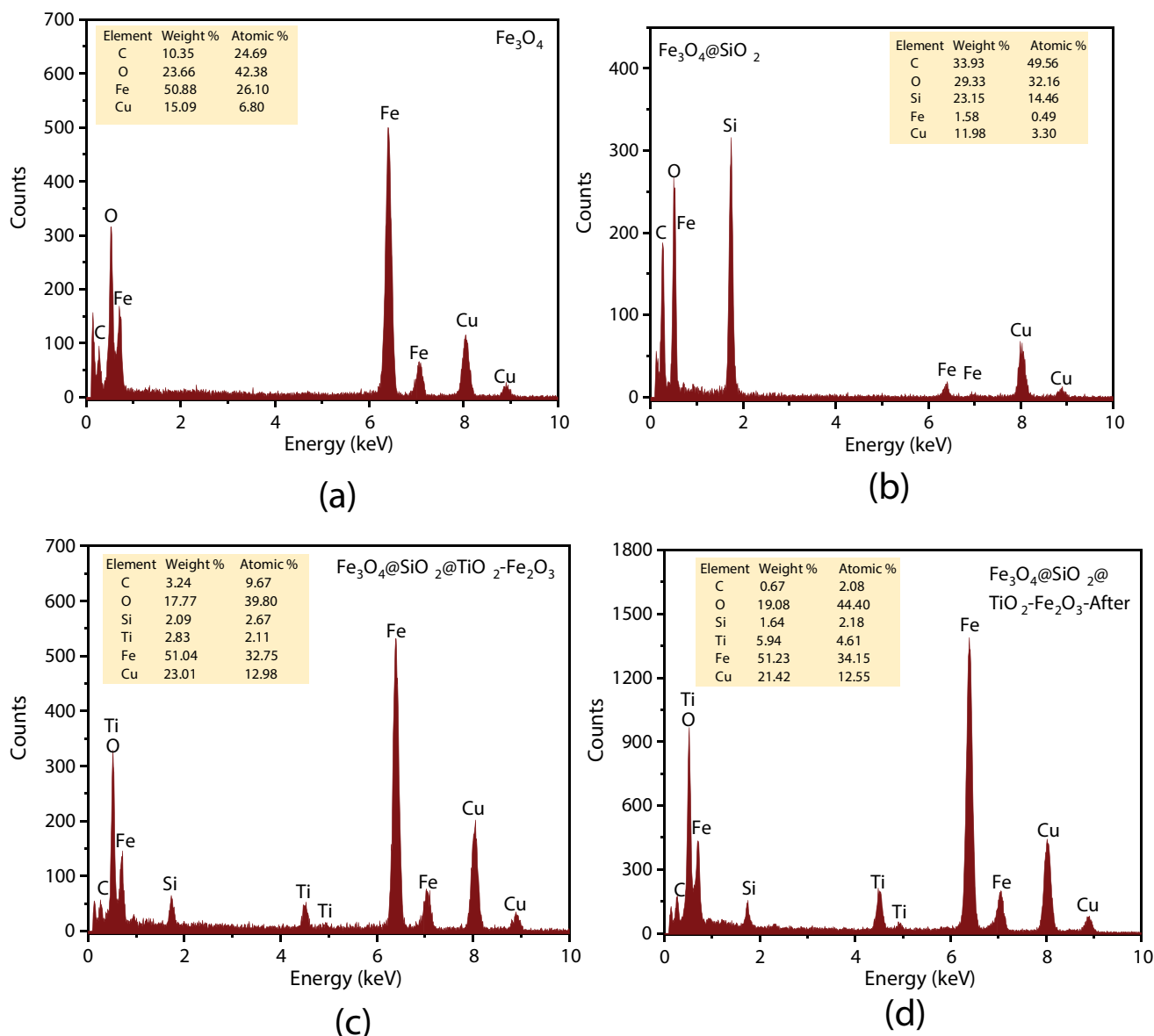
Fig. 6. XRF of Fe$_3$O$_4$, Fe$_3$O$_4$@SiO$_2$, Fe$_3$O$_4$@SiO$_2$@TiO$_2$-Fe$_2$O$_3$ and Fe$_3$O$_4$@SiO$_2$@TiO$_2$-Fe$_2$O$_3$ magnetic particles degradation of phenol.

recombination was inhibited and the photocatalytic activity of the composite was enhanced [42,43]. Under xenon illumination, the TiO$_2$-Fe$_2$O$_3$ nanoparticles encrusted on Fe$_3$O$_4$@SiO$_2$ to absorb photon energy, which can facilitate the electrons transfer from the valence band (VB) to conduction band (CB), correspondingly generating photo-induced electron–hole pairs. Unluckily, the photogenerated electron-hole pairs can only exist for a few nanoseconds, which will severely induce the recombination of photo-induced electrons (e$^-$) and holes (h$^+$), thereby decreasing the photocatalytic performance [44,45]. Fortunately, the presence of TiO$_2$-Fe$_2$O$_3$ can provide more transmission channels for electrons, promoting the transfer of photo-generated electrons from TiO$_2$-Fe$_2$O$_3$ CB to Fe$_3$O$_4$@SiO$_2$ surface, which can efficiently reduce the electron-hole recombination rate, eventually enhancing the photocatalytic property of the Fe$_3$O$_4$@SiO$_2$@TiO$_2$-Fe$_2$O$_3$ binary nanocomposite. The photo-generated electrons are easily trapped by the oxygen dissolved in water to generate O$_2^{\bullet-}$ due to superior oxidation [46,47]. In addition, the photo-induced holes can directly oxidize organic components adsorbed on the photocatalyst surface or react with adsorbed OH$^-$ groups or H$_2$O molecules to produce hydroxyl radicals ($^\bullet$OH) who possess the strongest oxidizing ability among the oxidants present in the water, which can easily oxidize the majority of inorganic and organic contaminants in wastewater. The photocatalytic degradation mechanism of phenol can be illustrated by the following equations:

$$TiO_2 + h\nu \rightarrow h^+ + e^- \tag{2}$$

$$e^- + O_2 \rightarrow O_2^{\bullet-} \tag{3}$$

$$h^+ + OH^{\bullet-} \rightarrow OH^{\bullet} \tag{4}$$

$$Phenol + O_2^{\bullet-} + {}^{\bullet}OH + h^+ \rightarrow nCO_2 + H_2O \tag{5}$$

4. Conclusions

The major goal of this study was to synthesize, characterize, and assess the photocatalytic activity of $Fe_3O_4@SiO_2@TiO_2\text{-}Fe_2O_3$. Ultrasonic-assisted co-precipitation and sol–gel anaerobic calcination were used to create core-shell nanomaterial photocatalysts. Photocatalysts were made and tested under various experimental circumstances in order to identify the optimum condition and achieve the higher photocatalytic performance.

Under strong alkalinity conditions, the optimized $Fe_3O_4@SiO_2@TiO_2\text{-}Fe_2O_3$ nanohybrid could degrade 41.51% of phenol from aqueous solution when exposed to xenon light. As the Fe_2O_3 concentration of the samples grew, the band gaps of the $TiO_2\text{-}Fe_2O_3$ photocatalysts decreased. This results in the photocatalytic oxidation of phenol in the visible light area, with $Fe_3O_4@SiO_2@TiO_2\text{-}Fe_2O_3$ composites acting as photocatalysts, which might be a promising contender for wastewater purification.

Data availability statement

Some or all data that support the findings of this study are available from the corresponding author upon reasonable request.

Acknowledgement

Conflict of interest statement

None.

References

[1] H.Y. Fan, G.Y. Yi, Z.T. Zhang, X.X. Zhang, P. Li, C.X. Zhang, L.J. Chen, Y.L. Zhang, Q. Sun, Binary TiO_2/RGO photocatalyst for enhanced degradation of phenol and its application in underground coal gasification wastewater treatment, Opt. Mater., 120 (2021) 111482, doi: 10.1016/j.optmat.2021.111482.

[2] O. Amina, M. Sara, P. Senthil Kumar, K. Ashish, P. Velayudhaperumal Chellam, Ö. Gökkuş, Agricultural waste materials for adsorptive removal of phenols, chromium(VI) and cadmium(II) from wastewater: a review, Environ. Res., 204 (2022) 111916, doi: 10.1016/j.envres.2021.111916.

[3] S. Mohammadi, A. Kargari, H. Sanaeepur, K. Abbassian, A. Najafi, E. Mofarrah, Phenol removal from industrial wastewaters: a short review, Desal. Water Treat., 53 (2015) 2215–2234.

[4] M. Alshabib, S.A. Onaizi, A review on phenolic wastewater remediation using homogeneous and heterogeneous enzymatic processes: current status and potential challenges, Sep. Purif. Technol., 219 (2019) 186–207.

[5] P. Muthamilselvi, R. Karthikeyan, A. Kapoor, S. Prabhakar, Continuous fixed-bed studies for adsorptive remediation of phenol by garlic peel powder, Int. J. Ind. Chem., 9 (2018) 379–390.

[6] J. Wang, Q. Sui, S.L. Yu, Y. Huang, S. Huang, B. Wang, D. Xu, W. Zhao, M. Kong, Y. Zhang, S. Hou, G. Yu, Source apportionment of phenolic compounds based on a simultaneous monitoring of surface water and emission sources: a case study in a typical region adjacent to Taihu Lake watershed, Sci. Total Environ., 722 (2020) 137946, doi: 10.1016/j.scitotenv.2020.137946.

[7] A. Ribas-Agustí, O. Martín-Belloso, R. Soliva-Fortuny, P. Elez-Martínez, Food processing strategies to enhance phenolic compounds bioaccessibility and bioavailability in plant-based foods, Crit. Rev. Food Sci. Nutr., 58 (2018) 2531–2548.

[8] D. O'Connor, D. Hou, Y.S. Ok, Y. Song, A.K. Sarmah, X. Li, F.M.G. Tack, Sustainable in situ remediation of recalcitrant organic pollutants in groundwater with controlled release materials: a review, J. Controlled Release, 283 (2018) 200–213.

[9] A. Othmani, A. Kesraoui, H. Akrout, I. Elaissaoui, M. Seffen, Coupling anodic oxidation, biosorption and alternating current as alternative for wastewater purification, Chemosphere, 249 (2020a) 126480, doi: 10.1016/j.chemosphere.2020.126480.

[10] A. Doggaz, A. Attour, M. Le Page Mostefa, K. Côme, M. Tlili, F. Lapicque, Removal of heavy metals by electrocoagulation from hydrogenocarbonate-containing waters: compared cases of divalent iron and zinc cations, J. Water Process Eng., 29 (2019) 100796, doi: 10.1016/j.jwpe.2019.100796.

[11] S.Q. Wu, X.J. Tan, K. Liu, J.Y. Lei, L.Z. Wang, J.L. Zhang, TiO_2 (B) nanotubes with ultrathin shell for highly efficient photocatalytic fixation of nitrogen, Catal. Today, 335 (2019) 214–220.

[12] S. Garcia-Segura, J. Keller, E. Brillas, J. Radjenovic, Removal of organic contaminants from secondary effluent by anodic oxidation with a boron-doped diamond anode as tertiary treatment, J. Hazard. Mater., 283 (2015) 551–557.

[13] E. Poonguzhali, A. Kapoor, P. Senthil Kumar, S. Prabhakar, Effective separation of toxic phenol from aquatic system using membrane assisted solvent extraction system, Desal. Water Treat., 221 (2021) 316–327.

[14] J. Theerthagiri, S.J. Lee, K. Karuppasamy, S. Arulmani, S. Veeralakshmi, M. Ashokkumar, M.Y. Choi, Application of advanced materials in sonophotocatalytic processes for the remediation of environmental pollutants, J. Hazard. Mater., 412 (2021) 125245, doi: 10.1016/j.jhazmat.2021.125245.

[15] W. Min, L. Jiajun, X. Chuang, F. Li, Sonocatalysis and sonophotocatalysis in $CaCu_3Ti_4O_{12}$ ceramics, Ceram. Int., 48 (2022) 11338–11345.

[16] S. Ledys Copete-Pertuz, A. Efraím Serna-Galvis, P. Jersson, A. Ricardo Torres-Palma, L. Amanda Mora-Martínez, Coupling chemical oxidation processes and *Leptosphaerulina* sp. mycoremediation to enhance the removal of recalcitrant organic pollutants in aqueous systems, Sci. Total Environ., 772 (2021) 145449, doi: 10.1016/j.scitotenv.2021.145449.

[17] W. Zhang, Z. Yu, P. Rao, I.M.C. Lo, Uptake and toxicity studies of magnetic TiO_2-based nanophotocatalyst in *Arabidopsis thaliana*, Chemosphere, 224 (2019) 658–667.

[18] S. Feizpoor, A. Habibi-Yangjeh, Ternary TiO_2/Fe_3O_4/$CoWO_4$ nanocomposites: novel magnetic visible-light-driven photocatalysts with substantially enhanced activity through p-n heterojunction, J. Colloid Interface Sci., 524 (2018) 325–336.

[19] B. Yuzer, M. Guida, F. Ciner, B. Aktan, M. Iberia Aydin, S. Meric, H. Selcuk, A multifaceted aggregation and toxicity assessment study of sol–gel-based TiO_2 nanoparticles during textile wastewater treatment, Desal. Water Treat., 57 (2016) 4966–4973.

[20] V. Suba, M. Saravanabhavan, L.S. Krishna, S. Kaleemulla, E. Ranjith Kumar, G. Rathika, Evaluation of curcumin assistance in the antimicrobial and photocatalytic activity of a carbon based TiO_2 nanocomposite, New J. Chem., 44 (2020) 15895–15907.

[21] S. Tamilselvi, M. Asaithambi, P. Sivakumar, Nano-TiO_2-loaded activated carbon fiber composite for photodegradation of a textile dye, Desal. Water Treat., 57 (2014) 15495–15502.

[22] X.X. Zhang, Z. Peng, X.Q. Lu, Y. Lv, G.Y. Cai, L. Yang, Z.H. Dong, Microstructural evolution and biological performance of Cu-incorporated TiO_2 coating fabricated through

one-step micro-arc oxidation, Appl. Surf. Sci., 508 (2020) 144766, doi: 10.1016/j.apsusc.2019.144766.

[23] A. Balakrishnan, K. Gopalram, S. Appunni, Photocatalytic degradation of 2,4-dicholorophenoxyacetic acid by TiO$_2$ modified catalyst: kinetics and operating cost analysis, Environ. Sci. Pollut. Res., 28 (2021) 33331–33343.

[24] S.D. Perera, R.G. Mariano, K. Vu, N. Nour, O. Seitz, Y. Chabal, K.J. Balkus Jr., Hydrothermal synthesis of graphene-TiO$_2$ nanotube composites with enhanced photocatalytic activity, ACS Catal., 2 (2012) 949–956.

[25] Y.C. López, H. Viltres, N.K. Gupta, P. Acevedo-Peña, C. Leyva, Y. Ghaffari, A. Gupta, S. Kim, J. Bae, K.S. Kim, Transition metal-based metal–organic frameworks for environmental applications: a review, Environ. Chem. Lett., 19 (2021) 1295–1334.

[26] M. Tong, D. Sun, R. Zhang, H. Liu, R. Chen, Preparation of Si–α-Fe$_2$O$_3$/CdS composites with enhanced visible-light photocatalytic activity for *p*-nitrophenol degradation, J. Alloys Compd., 862 (2021) 158271, doi: 10.1016/j.jallcom.2020.158271.

[27] Q. Xiao, C. Chuntao, L. Jianbin, Q. Wei, Z. Lei, D.P. Sun, Engineered defect-rich TiO$_2$/g-C$_3$N$_4$ heterojunction: a visible light-driven photocatalyst for efficient degradation of phenolic wastewater, Chemosphere, 286 (2022) 131696, doi: 10.1016/j.chemosphere.2021.131696.

[28] S.Q. Wu, C.X. He, L.Z. Wang, J.L. Zhang, High-efficiency electron tandem flow mode on carbon nitride/titanium dioxide heterojunction for visible light nitrogen photofixation, Chem. Eng. J., 443 (2022) 136425, doi: 10.1016/j.cej.2022.136425.

[29] S. Wang, L.N. Bai, H.M. Sun, Q. Jiang, J.S. Lian, Structure and photocatalytic property of Mo-doped TiO$_2$ nanoparticles, Powder Technol., 244 (2013) 9–15.

[30] L.B. Shun, Z.X. Jian, The synergetic effect of V and Fe-co-doping in TiO$_2$ studied from the DFT + U first-principle calculation, Appl. Surf. Sci., 399 (2017) 654–662.

[31] Z.-Q. Li, H.-L. Wang, L.-Y. Zi, J.-J. Zhang, Y.-S. Zhang, Preparation and photocatalytic performance of magnetic TiO$_2$–Fe$_3$O$_4$/graphene (RGO) composites under VIS-light irradiation, Ceram. Int., 41 (2015) 10634–10643.

[32] F. Ghasemy-Piranloo, S. Dadashian, F. Bavarsiha, Fe$_3$O$_4$/SiO$_2$/TiO$_2$–Ag cubes with core/shell/shell nano-structure: synthesis, characterization and efficient photo-catalytic for phenol degradation, J. Mater. Sci.: Mater. Electron., 30 (2019) 12757–12768.

[33] D. Wang, J. Yang, X. Li, J. Wang, H. Zhai, J. Lang, H. Song, Effect of thickness and microstructure of TiO$_2$ shell on photocatalytic performance of magnetic separable Fe$_3$O$_4$/SiO$_2$/mTiO$_2$ core-shell composites, Phys. Status Solidi A, 214 (2017) 1600665, doi: 10.1002/pssa.201600665.

[34] P. Chanhom, N. Charoenlap, B. Tomapatanaget, N. Insin, Colloidal titania-silica-iron oxide nanocomposites and the effect from silica thickness on the photocatalytic and bactericidal activities, J. Magn. Magn. Mater., 427 (2017) 54–59.

[35] W. Zhao, S. Liu, S. Zhang, R. Wang, K. Wang, Preparation and visible-light photocatalytic activity of N-doped TiO$_2$ by plasma-assisted sol–gel method, Catal. Today, 337 (2019) 37–43.

[36] S.P. Onkani, P.N. Diagboya, F.M. Mtunzi, M.J. Klink, B.I. Olu-Owolabi, V. Pakade, Comparative study of the photocatalytic degradation of 2–chlorophenol under UV irradiation using pristine and Ag-doped species of TiO$_2$, ZnO and ZnS photocatalysts, J. Environ. Manage., 260 (2020) 110145, doi: 10.1016/j.jenvman.2020.110145.

[37] Y. Liu, S. Zhou, F. Yang, H. Qin, Y. Kong, Degradation of phenol in industrial wastewater over the F–Fe/TiO$_2$ photocatalysts under visible light illumination, Chin. J. Chem. Eng., 24 (2016) 1712–1718.

[38] A. Dixit, A.K. Mungray, M. Chakraborty, Photochemical oxidation of phenol and chlorophenol by UV/H$_2$O$_2$/TiO$_2$ process: a kinetic study, Int. J. Chem. Eng. Appl., 1 (2010) 247–250.

[39] B. MirzaHedayat, M. Noorisepehr, E. Dehghanifard, A. Esrafili, R. Norozi, Evaluation of photocatalytic degradation of 2,4-dinitrophenol from synthetic wastewater using Fe$_3$O$_4$@SiO$_2$@TiO$_2$/rGO magnetic nanoparticles, J. Mol. Liq., 264 (2018) 571–578.

[40] A. Banisharif, A.A. Khodadadi, Y. Mortazavi, A.A. Firooz, J. Beheshtian, S. Agah, S. Menbari, Highly active Fe$_2$O$_3$-doped TiO$_2$ photocatalyst for degradation of trichloroethylene in air under UV and visible light irradiation: experimental and computational studies, Appl. Catal., B, 165 (2015) 209–221.

[41] J.A. Navío, G. Colón, M.I. Litter, G.N. Bianco, Synthesis, characterization and photocatalytic properties of iron-doped titania semiconductors prepared from TiO$_2$ and iron(III) acetylacetonate, J. Mol. Catal. A: Chem., 106 (1996) 267–276.

[42] F. Ghasemy-Piranloo, S. Dadashian, F. Bavarsiha, Fe$_3$O$_4$/SiO$_2$/TiO$_2$–Ag cubes with core/shell/shell nano-structure: synthesis, characterization and efficient photo-catalytic for phenol degradation. J. Mater. Sci.: Mater. Electron., 30 (2019) 12757–12768.

[43] H. Kiziltaş, T. Tekin, D. Tekin, Preparation and characterization of recyclable Fe$_3$O$_4$@SiO$_2$@TiO$_2$ composite photocatalyst, and investigation of the photocatalytic activity, Chem. Eng. Commun., 208 (2021) 1041–1053.

[44] S. Banerjee, P. Benjwal, M. Singh, K.K. Kar, Graphene oxide (rGO)-metal oxide (TiO$_2$/Fe$_3$O$_4$) based nanocomposites for the removal of methylene blue, Appl. Surf. Sci., 439 (2018) 560–568.

[45] H. Zhang, X. Lv, X. Li, Y. Wang, J. Li, P25-Graphene composite as a high performance photocatalyst, ACS Nano, 4 (2010) 380–386.

[46] Y. Dai, Y. Jing, J. Zeng, Q. Qi, C. Wang, D. Goldfeld, C. Xu, Y. Zheng, Y. Sun, Nanocables composed of anatase nanofibers wrapped in UV-light reduced graphene oxide and their enhancement of photoinduced electron transfer in photoanodes, J. Mater. Chem., 21 (2011) 18174–18179.

[47] B. Jiang, C. Tian, Q. Pan, Z. Jiang, J.-Q. Wang, W. Yan, H. Fu, Enhanced photocatalytic activity and electron transfer mechanisms of graphene/TiO$_2$ with exposed {001} facets, J. Phys. Chem. C, 115 (2011) 23718–23725.